Hindawi Publishing Corporation
Journal of Fluids
Volume 2016, Article ID 4931426, 10 pages
http://dx.doi.org/10.1155/2016/4931426

Research Article

Effect of Yield Power Law Fluid Rheological Properties on Cuttings Transport in Eccentric Horizontal Narrow Annulus

Titus Ntow Ofei

Petroleum Engineering Department, Universiti Teknologi PETRONAS, Bandar Seri Iskandar, 32610 Tronoh, Malaysia

Correspondence should be addressed to Titus Ntow Ofei; titusofei@hotmail.com

Received 8 March 2016; Revised 5 May 2016; Accepted 6 June 2016

Academic Editor: Bhim C. Meikap

Narrow annular drilling such as casing-while-drilling technique is gaining popularity due to its ability to mitigate nonproductive time during oil and gas drilling operations. However, very little is known about the flow dynamics in narrow annular drilling. In this study, the Eulerian-Eulerian two-fluid model was used to examine the influence of Yield Power Law fluid rheological properties on cuttings transport in eccentric horizontal narrow annulus. The flow was assumed as fully developed, laminar, and transient state. The present simulation model was validated against experimental data, where a mean percent error of –1.2% was recorded. Results revealed an increase in the radial distribution of cuttings transport velocity in the wide annular region as the consistency index, K, and the flow behavior index, n, increase. Nonetheless, increasing the yield stress, τ_o, had insignificant effect on the cuttings transport velocity. Three-dimensional profiles showed how cuttings preferred to travel in less resistant flow area, whereas cuttings concentration builds up in the narrow annular region. Furthermore, annular frictional pressure losses also increased as K, n, and τ_o increased. This study serves as a guide to properly optimize drilling fluid rheological properties for efficient cuttings transport and equivalent circulating density (ECD) management in narrow annular drilling.

1. Introduction

Drilling fluid rheological properties are important parameters which contribute to effective hole cleaning. Adari et al. [1] indicated that drilling fluid rheological properties are highly influential on cuttings transport; hence, care must be taken in predicting the optimum parameters to enhance better hole cleaning. The Herschel-Bulkley (HB) viscosity model, also called Yield Power Law (YPL) model, is known to correlate better to the drilling fluid viscosity curve than most other rheological models [2, 3].

In literature, most experimental studies on drilling fluids observed that the drilling fluid rheological curves (rheogram) conformed best to that of YPL fluid model. Ahmed and Miska [4] conducted extensive experimental study with polymer-based fluids in concentric and eccentric horizontal annuli without the presence of cuttings. The fluid rheological properties were accurately characterized using YPL model. The effects of inner pipe rotation, eccentricity, and flow rates on frictional pressure losses were analyzed. Other experimental studies [5–8] also accurately fitted their fluid rheological parameters using the Yield Power Law model. The authors proposed pressure loss equations for YPL fluid flow in pipes and annuli which is an integration of analytical, semianalytical, and empirical equations for laminar, transitional, and turbulent flows. Taghipour et al. [9] were among the first researchers to use YPL fluids to perform cuttings transport experimental study in inclined and horizontal annulus of diameter ratio, $\kappa = 0.50$. They measured annular pressure losses, solids bed height, and drill string torque.

Several experimental and numerical studies have also evaluated the effects of drilling fluid rheological properties on cuttings transport. Cho et al. [10] observed that a decrease in flow behavior index, n, resulted in a decrease of stationary bed, whereas moving bed layer increases. Adari et al. [1] also observed that the increase in the ratio of flow behavior index to consistency index (n/K) reduced cuttings bed height. In addition, the drilling fluid yield stress (YS) and plastic

viscosity (PV) also influenced cuttings removal. Valluri et al. [11] presented their experimental findings that an increase in YS at constant flow rate without drillpipe rotation resulted in negligible cuttings bed erosion. Furthermore, Mohammadsalehi and Malekzadeh [12] also observed that a reduction in PV and YS resulted in a better hole cleaning at reduced flow rates. Horton et al. [13] explored how rheological properties of YPL fluids, bottomhole temperature, and fluid configuration in the wellbore affect the temperature profile in deep offshore wells. It was concluded that the yield stress, τ_o, value is the most important parameter that significantly affects the shut-in time for the well to cool to 68°F, while the flow behavior index, n, and consistency index, K, have minor effect on both oil-based and water-based YPL fluids.

In addition, other authors have utilized CFD approach to model YPL fluid through pipes and annuli. Bui [14] conducted a CFD study of YPL fluid flowing through pipes and concentric and eccentric annuli with tool joints. The author examined the effects of drillpipe rotation and tool joint on annular pressure losses. Ofei et al. [15] also employed CFD technique to model YPL fluid flowing in both concentric and eccentric narrow annuli. The authors analyzed the effects of bulk velocity, diameter ratio, inner pipe rotation speed, and eccentricity on the radial distributions of axial and tangential flow profiles. Mokhtari et al. [16] carried out CFD study to simulate the effects of YPL fluid rheological parameters on pressure losses in eccentric annulus. The authors established that an increase in the fluid yield stress, τ_o, increases the pressure loss substantially and creates a wider plug zone velocity. Furthermore, they indicated that as the fluid becomes more shear thinning, pressure loss decreases considerably.

It is evident that very rare or few studies on cuttings transport using YPL fluids exist in literature. As the oil and gas industries are developing the interest in the use of YPL fluids in drilling operations, there is need to conduct more research to understand the behavior of this fluid of interest on cuttings transport.

Several studies [17–28] have adopted CFD techniques to model solid-liquid flow in annular geometries with much accuracy. This is due to the many advantages CFD has over experimental setup and empirical correlations in handling complex multiphase flow problems with unlimited physical and operational conditions.

The present study adopts the inhomogeneous Eulerian-Eulerian two-fluid model to analyze the effect of fluid rheological properties on cuttings-YPL flow in eccentric narrow horizontal annulus. A finite volume method is used to solve the continuity and momentum equations. CFD methods have been proven to be very effective for multiphase flow problems due to their ability in handling unlimited number of physical and operational conditions as well as eliminating the need for expensive experimental and materials setups.

Within the context of this study, the radial distributions of cuttings transport velocity were observed in both wide and narrow annular regions. The wide region (sector A-A) is the gap between the top of the drillpipe and hole, while the gap between the bottom of the drillpipe and hole represents the narrow region (sector B-B) as shown in Figure 1.

2. Materials and Methods

The inhomogeneous (Eulerian-Eulerian) two-fluid model in ANSYS CFX 14.0, where both the liquid and solid phases are considered interpenetrating continua, is adopted in this study. Other models such as Eulerian-Lagrangian model, however, simulate the solid phase as a discrete phase and allows for particle tracking. The Eulerian-Eulerian model is preferred to the Eulerian-Lagrangian model due to its ability to handle high solid volume fractions. Furthermore, it accounts for particle-particle interaction and includes turbulence automatically. A drawback of this model is, however, the need for complex closure relations. The commercial software package ANSYS CFX 14.0 consists of the following five (5) specialized components: (a) DesignModeler for building the geometries, (b) CFX Mesh for mesh generation (c) CFX-Pre for flow model definition, (d) CFX-Solver for solving the governing equations, and (e) CFX-Post for analyzing the results. The following continuity and momentum equations representing the two-phase flow model are described for the sake of brevity.

2.1. Governing Equations. The solid-liquid flow is assumed as (a) isothermal and (b) laminar and transient state.

2.1.1. Continuity Equations. The governing continuity equations for both liquid and solid phases could be expressed, respectively, as [29]

$$\begin{aligned} \frac{\partial}{\partial t}\left(\hbar_l\right) + \nabla\left(\hbar_l U_l\right) &= 0, \\ \frac{\partial}{\partial t}\left(\hbar_s\right) + \nabla\left(\hbar_s U_s\right) &= 0, \end{aligned} \tag{1}$$

where the solid and liquid phase volume fractions sum up to unity as

$$\hbar_s + \hbar_l = 1. \tag{2}$$

2.1.2. Momentum Equations. The forces acting on each phase and interphase momentum transfer term that models the interaction between each phase are given below [29].

For liquid phase,

$$\begin{aligned} &\rho_l \hbar_l \left[\frac{\partial U_l}{\partial t} + U_l \cdot \nabla U_l\right] \\ &\quad = -\hbar_l \nabla p + \hbar_l \nabla \cdot \overline{\overline{\tau}}_l + \hbar_l \rho_l g - M. \end{aligned} \tag{3}$$

Similarly, for solid phase,

$$\begin{aligned} &\rho_s \hbar_s \left[\frac{\partial U_s}{\partial t} + U_s \cdot \nabla U_s\right] \\ &\quad = -\hbar_s \nabla p + \hbar_s \nabla \cdot \overline{\overline{\tau}}_l + \nabla \cdot \overline{\overline{\tau}}_s - \nabla P_s + \hbar_s \rho_s g + M. \end{aligned} \tag{4}$$

2.2. Other Closure Models

2.2.1. Interphase Drag Force Model. Considering spherical particles, the drag force per unit volume is given as

$$M_d = \frac{3C_D}{4d_s} \hbar_s \rho_l \left|U_s - U_l\right| \left(U_s - U_l\right). \tag{5}$$

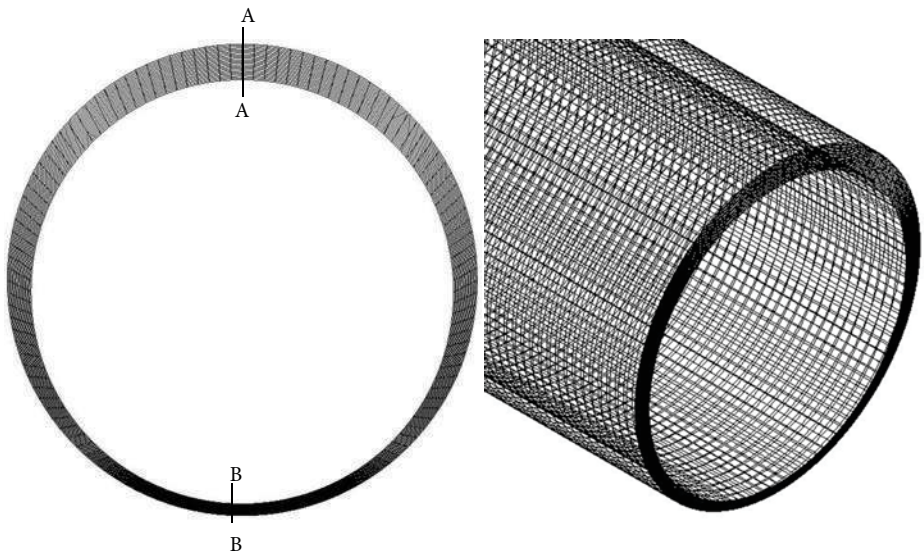

Figure 1: 2D and 3D meshed sections of eccentric horizontal annular geometry.

For densely distributed solid particles, where the solid volume fraction $\kappa_s < 0.2$, the drag coefficient model by Wen-Yu [30] may be utilized. This model is modified and implemented in ANSYS CFX 14.0 to ensure the correct limiting behavior in the inertial regime as

$$C_D = \kappa_l^{-1.65} \max\left[\frac{24}{N'_{\mathrm{Re}_p}}\left(1 + 0.15 N'^{0.687}_{\mathrm{Re}_p}\right), 0.44\right], \quad (6)$$

where $N'_{\mathrm{Re}_p} = \kappa_l N_{\mathrm{Re}_p}$ and $N_{\mathrm{Re}_p} = \rho_l |U_l - U_s| d_s / \mu_l$.

For large solid volume fraction, $\kappa_s > 0.2$, the drag model by Gidaspow [31] may be used with the interphase drag force per unit volume defined as

$$M_d = \frac{150\left(1-\kappa_l\right)^2 \mu_l}{\kappa_l d_s^2} + \frac{7}{4}\frac{\left(1-\kappa_l\right)\rho_l \left|U_l - U_s\right|}{d_s}. \quad (7)$$

2.2.2. Lift Force Model. For spherical solid particles, ANSYS CFX employs the lift force model by Saffman [32, 33] as

$$M_L = \frac{3}{2\pi}\frac{\sqrt{\nu_l}}{d_s\sqrt{\left|\nabla \times U_l\right|}} C'_L \kappa_s \rho_l \left(U_s - U_l\right)\left(\nabla \times U_l + 2\Omega\right). \quad (8)$$

The authors correlated the lift force for low Reynolds number past a spherical solid particle, where $C'_L = 6.46$ and $0 \le N_{\mathrm{Re}_p} \le N_{\mathrm{Re}_\omega} \le 1$. For higher range of solid particle Reynolds number, Saffman's correlation was generalized by Mei and Klausner [34] as

$$C'_L = \begin{cases} 6.46 \cdot f\left(N_{\mathrm{Re}_p}, N_{\mathrm{Re}_\omega}\right), & \text{for: } N_{\mathrm{Re}_p} < 40, \\ 6.46 \cdot 0.0524 \cdot \left(\beta N_{\mathrm{Re}_p}\right)^{1/2}, & \text{for: } 40 < N_{\mathrm{Re}_p} < 100, \end{cases} \quad (9)$$

where $\beta = 0.5(N_{\mathrm{Re}_\omega}/N_{\mathrm{Re}_p})$, and

$$f\left(N_{\mathrm{Re}_p}, N_{\mathrm{Re}_\omega}\right) = \left(1 - 0.3314\beta^{0.5}\right)\cdot \exp\left(-0.1 N_{\mathrm{Re}_p}\right) + 0.3314\beta^{0.5} \quad (10)$$

and $N_{\mathrm{Re}_\omega} = \rho_l \omega_l d_s^2 / \mu_l$, $\omega_l = |\nabla \times U_l|$.

2.3. Solid Phase Viscosity Model. Solid particles suspended in a liquid phase are affected by shear rate redistribution. The solid phase viscosity, μ_s, is related to the apparent suspension viscosity, μ_{susp}, and liquid apparent viscosity, μ_a, as

$$\mu_s = \frac{\mu_{\mathrm{susp}} - \left(1-\kappa_s\right)\mu_a}{\kappa_s}. \quad (11)$$

The suspension viscosity is expressed in terms of relative viscosity, μ_r, as

$$\mu_{\mathrm{susp}} = \mu_r \mu_a. \quad (12)$$

The relative viscosity of more concentrated suspension with particle-particle interactions is given by [35]

$$\mu_r = 1 + 2.5\kappa_s + 10.05\kappa_s^2 + 0.00273\exp\left(16.6\kappa_s\right). \quad (13)$$

The first two terms of (13) represent Einstein [36] equation.

Equations (11) to (13) are coded into CFX library as expression language to compute the solid viscosity.

2.4. Carrier Fluid Viscosity. There is singularity problem associated with the classical YPL viscosity model at vanishing shear rate. To alleviate this, the proposed YPL viscosity function by Mendes and Dutra [37] is implemented in the present CFD study as

$$\eta\left(\dot{\gamma}\right) = \left(1 - \exp\left(\frac{-\eta_o\left|\dot{\gamma}\right|}{\tau_o}\right)\right)\left(\frac{\tau_o}{\left|\dot{\gamma}\right|} + K\left|\dot{\gamma}\right|^{n-1}\right). \quad (14)$$

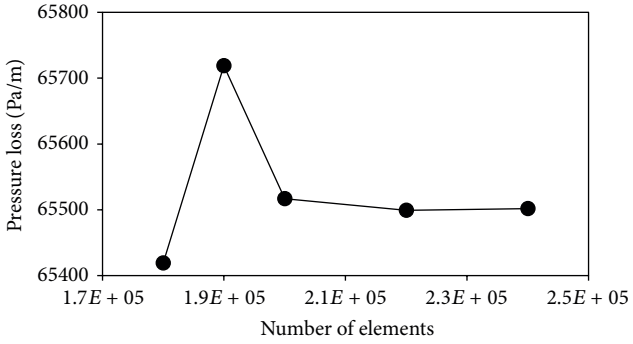

Figure 2: Grid independent study.

This viscosity function is numerically stable and devoid of discontinuity. Equation (14) is currently not available in the library of variables of ANSYS CFX 14.0; hence, it is modeled as expression language and coupled with the momentum equations.

2.5. Boundary Conditions and Meshing. At the inlet, a mass flow rate is specified, while a zero-gauge pressure is specified at the outlet boundary. At the pipe walls, different boundary conditions were used for both liquid and solids. The usual no-slip condition was imposed at the walls for the liquid phase, while for the solid phase, the free-slip condition was assumed at the walls to prevent the solid phase from adhering to the walls. This is consistent with real flow behavior of solid particles flowing near a solid boundary. The solid volume fraction in the domain was specified at the beginning of each simulation to correspond to the desired solid loading.

The annular 3D geometry of diameter ratio $\kappa = 0.90$ was meshed into structured hexahedral grids of approximately 2.4×10^5 elements. Grid independent study of numerical results of pressure losses were carried out until variations in results were insignificant. In this study, the optimum grid sizes used for the radial, circumferential, and axial directions are $20(r) \times 120(\theta) \times 100(z)$. Figure 1 shows a section of the 2D and 3D annular mesh, while Figure 2 depicts the results from the grid independence study.

2.6. Description of Simulation Study. The simulation of the two-phase solid-liquid flow was set up in three dimensions using ANSYS CFX 14.0 with the transport equations solved using CFX-Solver. The geometry dimensions, fluid rheological properties, solid properties, and operating parameters are presented in Table 1. To achieve a fully developed flow, the annular length, L, must be longer than the hydrodynamic entrance length L_h of the flow. In single-phase Newtonian fluids flowing in pipes, the hydrodynamic entrance length is presented as [38]

$$L_h = 0.05 N_{\mathrm{Re}} (D). \tag{15}$$

However, for a two-phase flow in annular gap with a non-Newtonian fluid, such expression as in (15) does not exist in literature. As a rule of thumb, the author adopted (15) by replacing the pipe diameter D with a hydraulic diameter $D_h = D_o - D_i$. It should be noted that a much longer annular length would only result in a longer simulation run.

Table 1: CFD simulation matrix.

Simulation data	Diameter ratio ($\kappa = D_i/D_o = 0.90$)
Flow behavior index (n)	0.31–0.75
Consistency index (K, Pa·s^n)	1.7–6.3
Yield stress (τ_o, Pa)	2–8
Zero shear rate viscosity (η_o, Pa·s)	1100
Fluid density (ρ_l, kg/m^3)	1020
Bulk fluid velocity (V_b, m/s)	0.50
Inner pipe rotation speed (ω, rpm)	0
Outer diameter (D_o, mm)	50.8
Inner diameter (D_i, mm)	45.7
Eccentricity ($\varepsilon = 2e/(D_o - D_i)$)	0.50
Cuttings density (ρ_s, kg/m^3)	2650
Avg. cuttings size (mm)	1.0 & 4.0
Rate of penetration, ROP (m/s)	0.00508

The CFX-Solver is based on a finite volume method in which the flow equations are integrated over each control volume. The advection scheme is set to high resolution to satisfy both accuracy and boundedness, where the blend factor, Γ, is computed locally to be close to 1 without resulting in nonphysical values. The algorithm by Rhie and Chow [39] is used to solve the pressure-velocity coupling, since it can overcome pressure-velocity oscillations.

It should be noted that the complexity of the transport equations could not permit numerical convergence under steady state. However, all simulations were run in transient state. It is usually recommended that simulation of such steady state nature should first be run under transient state when it is difficult to attain convergence [23]. A very small time step of 2.0×10^{-5} s was used in all simulations to help the solution converge; hence, the solutions finally converged when the convergence criterion was met at a root mean square (RMS) value of 10^{-4}. An average of 200 time steps was required to achieve convergence with 1–10 loop iterations at each time step.

2.7. Validation of Simulation Model. There is scarcity of data for cuttings transport study using YPL fluids. The most recent and only experimental cuttings transport study is conducted by Taghipour et al., where annular pressure losses were measured for cuttings-YPL fluid flow in inclined (30°) eccentric wellbore and are used to validate the two-phase CFD model. To validate the present model, the author simulated the experimental condition as presented by Taghipour et al. [9]. Table 2 presents the experimental setup with operational and rheological parameters. It is worth noting that only a section of the experimental flow loop length of 12 m was simulated. A simulated length of $100 \times (D_o - D_i)$ was chosen based on the calculated hydrodynamic length in (15) to ensure a fully developed flow as well as saving computational time. The flow was assumed as laminar and isothermal, while the drag and

Table 2: Experimental setup and operating conditions [9].

Inner diameter of casing, D_o, mm	101.6
Outer diameter of pipe, D_i, mm	50.8
Length of test section, L, m	12
Fluid density, ρ_l, kg/m^3	1020
Cutting density, ρ_s, kg/m^3	2400
Avg. cutting diameter, d_s, mm	1.25
Cutting injection rate, kg/s	0.05
Flow behaviour index, n	0.61
Fluid consistency index, K, Pa·s^n	0.09
Fluid yield stress, τ_o, Pa	1.3
Avg. fluid velocity, m/s	0.54–1.3
Drillpipe rotation speed, rpm	0

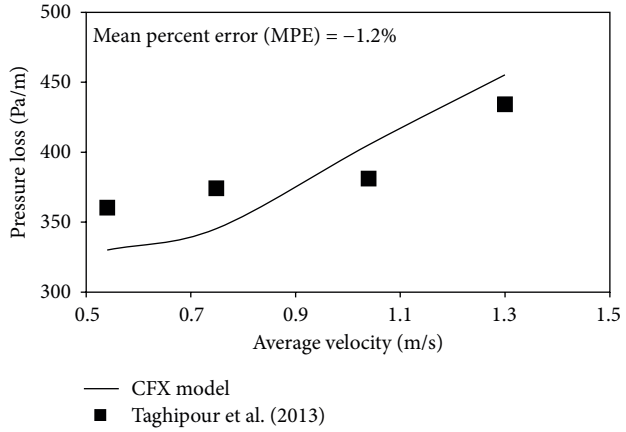

Figure 3: Experimental and simulation comparison of pressure loss data.

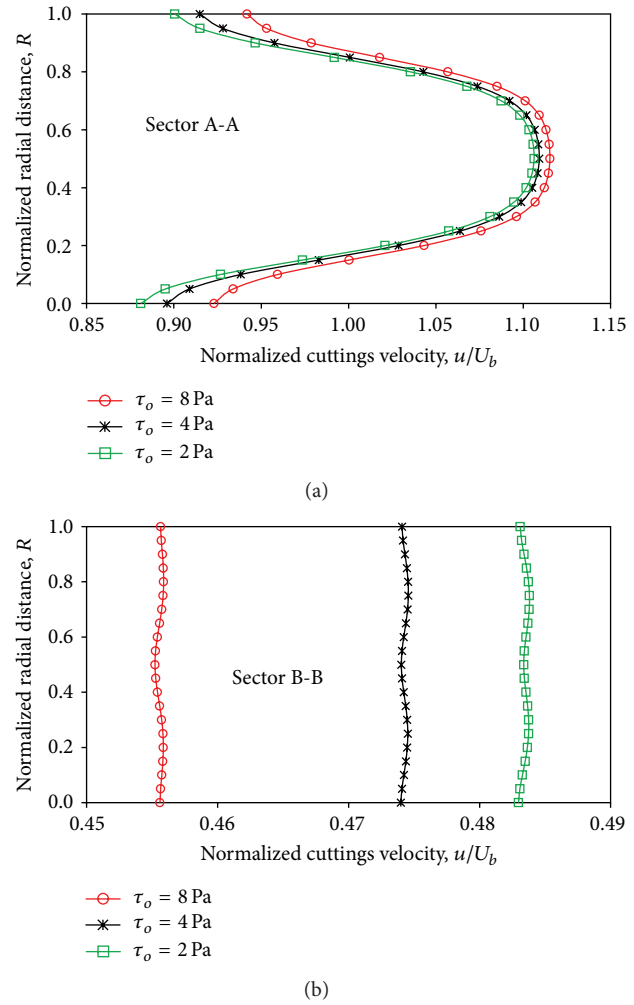

Figure 4: Effect of yield stress on cuttings transport velocity: (a) wide annular region and (b) narrow annular region.

lift forces were modelled using the models by Wen-Yu and Saffman as presented by (5) and (8), respectively. Figure 3 depicts the comparison between experimental and simulated pressure loss data. The comparison shows good agreement with a mean percentage error (MPE) between the calculated and measured pressure loss data of −1.2%, thus confirming the validity of the current model setup.

3. Results and Discussion

The simulation results reported here include the effects of yield stress, consistency index, and flow behavior index on cuttings transport velocity in YPL fluid in eccentric horizontal narrow annulus. Measurements of the radial distributions of the cuttings velocity profiles were taken along sectors A-A and B-B or at the positions 0° and 180° (see Figure 1), representing the wide and narrow regions of the eccentric wellbore, respectively. To generate the cuttings velocity profiles in CFX-Post, a plane was first created parallel to the symmetry of the wellbore. Secondly, a polyline was also created with a boundary intersection method, where the boundary list of wellbore outlet was intersected with the plane. Finally, a chart was chosen where the velocity profiles were plotted using the polyline.

Studies have shown that YPL fluids used in the field have a wide range of values of rheological properties. These rheological properties could include the following range of values [13]: yield stress, τ_o = 0.048–50.06 Pa, consistency index, K = 0.043–10.27 Pa·s^n, and flow behavior index, n = 0.314–0.978. The range of rheological parameters used in this study is within the aforementioned range of values usually encountered during drilling operation using YPL fluids.

3.1. Yield Stress, τ_o, Effect on Cuttings Transport Velocity. The yield stress value evaluates the ability of the drilling fluid to suspend drilled cuttings during circulation. A high yield stress fluid is believed to transport cuttings better than fluid with low yield stress having similar density values. Figures 4(a) and 4(b) depict the effect of yield stress on the radial distributions of cuttings transport velocity in both wide and narrow annular regions, respectively. Figure 4(a) shows that cuttings transport velocity increases with increasing

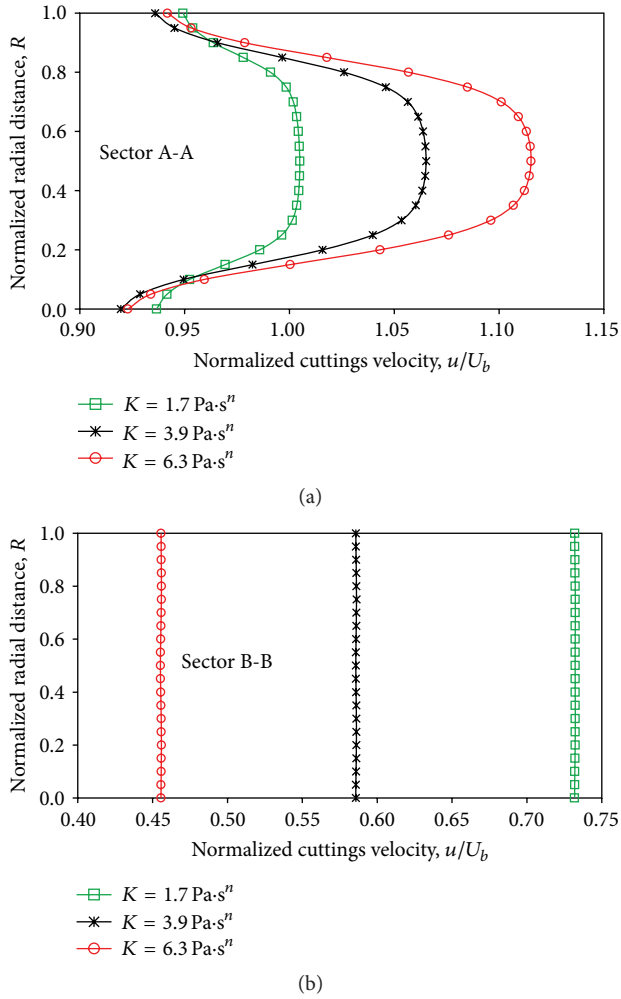

FIGURE 5: Effect of consistency index on cuttings transport velocity: (a) wide region and (b) narrow region.

yield stress in the wide annular region. This is an indication of better carrying capacity of high yield stress fluids. Nonetheless, this improvement in cuttings transport velocity is less significant especially in the core region as yield stress increases. In contrast, the narrow annular region provides greater flow resistance to high yield stress fluids, thus the least to transport cuttings, as shown in Figure 4(b). In the wide annular region (sector A-A), increasing τ_o from 2 to 8 Pa led to ~0.8% increment in the maximum cuttings velocity, whereas ~5.8% reduction in cuttings velocity occurred as τ_o increases from 2 to 8 Pa in the narrow annular region (sector B-B).

3.2. Consistency Index, K, Effect on Cuttings Transport Velocity. The consistency index of a drilling fluid is a rheological property related to the cohesion of the individual particles of the fluid, its ability to deform, and its resistance to flow. Figures 5(a) and 5(b) illustrate the consistency index's effect on cuttings transport velocity in both wide and narrow annular regions, respectively. It is observed in Figure 5(a), that is, in the wide annular region, that when all other parameters are kept constant, increasing K results in an increase in cuttings velocity.

It should be noted that K is directly proportional to the fluid's effective viscosity. Therefore, cuttings will travel less in low K fluids with low effective viscosity as the cuttings tend to settle faster at the bottom of the annulus due to gravity. Whereas in high K fluids, having high effective viscosity, cuttings will suspend for a longer period and, hence, travel faster and farther.

On the contrary, due to the flow restriction induced by the narrow annular region, cuttings travelling in high K fluids had the least velocity as opposed to those travelling in low K fluids (see Figure 5(b)). Investigations on the range of K values presented in this study show that increasing K from 1.7 to 6.3 Pa·s^n leads to ~11.0% increment in the maximum cuttings velocity in the wide annular region (sector A-A), whereas ~37.7% reduction in cuttings velocity was recorded as K increases from 1.7 to 6.3 Pa·s^n in the narrow annular region (sector B-B).

3.3. Flow Behavior Index, n, Effect on Cuttings Transport Velocity. The flow behavior index, n, is a measure of a fluid's shear-thinning performance in both pseudoplastic and yield stress fluids; that is, apparent viscosity decreases with increasing shear rate. Fluids with higher shear-thinning properties, $n < 1$, exhibit a plug (wider flat) flow region in the central core. Figures 6(a) and 6(b) demonstrate the effect of n on cuttings transport velocity in both wide and narrow annular regions, respectively. In the wide annular region, as shown in Figure 6(a), cuttings transport velocity in the fluid domain decreases as the fluid becomes more shear-thinning, especially in the core region. In the vicinity of the outer and inner pipe boundaries, high shear-thinning fluids exhibit a flat radial cuttings velocity profile. This increases the high velocity zone towards the boundaries with improved cuttings transport. Within the study range, increasing n from 0.31 to 0.75 led to increment of ~36.3% in the maximum cuttings velocity within the wide annular region (sector A-A) as shown in Figure 6(a). In the narrow annular region (sector B-B), cuttings travel faster in the radial distribution in low n fluids compared to high n fluids as shown in Figure 6(b). It is also observed that increasing n values from 0.31 to 0.75 led to a significant reduction in maximum cutting velocity by ~84.6%.

3.4. Three-Dimensional Cuttings Velocity and Concentration Profiles. Figure 7 presents the three-dimensional distributions of cuttings travelling in the annular geometry. Skewed cuttings velocity and concentration profiles were observed in the eccentric annulus as shown in Figures 7(a) and 7(b), respectively. These irregular distributions were due to the pipe-hole eccentricity which modified the flow by creating a high velocity zone in the wide annular region and a low or no velocity zone in the narrow annular region. The narrow region restricted the movement of the trapped cuttings and hence showed a very low velocity (see Figure 7(a)). Furthermore, high accumulation of cuttings bed can be observed in the narrow region of the annulus due to the effects of gravity and eccentricity as shown in Figure 7(b).

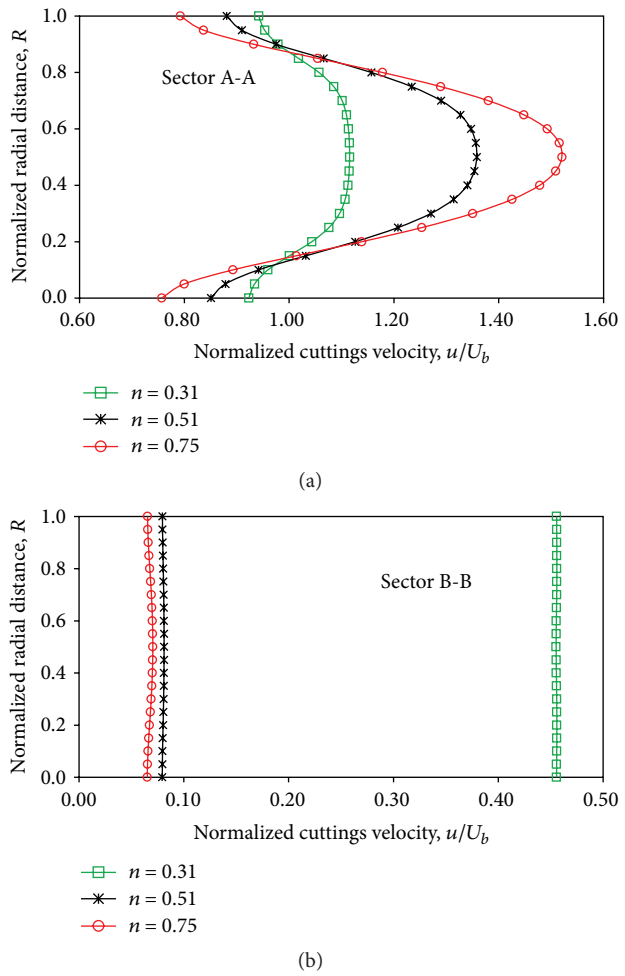

FIGURE 6: Effect of flow behavior index on cuttings transport velocity: (a) wide region and (b) narrow region.

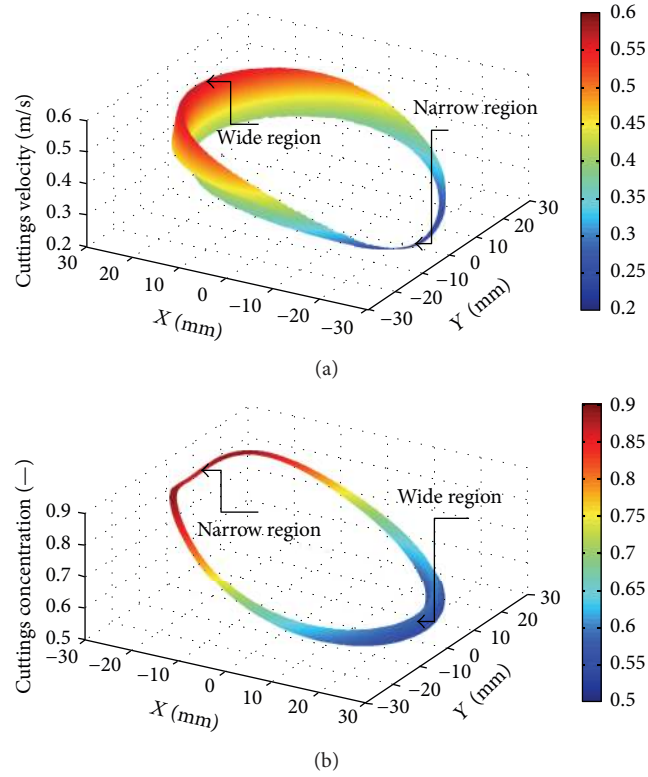

FIGURE 7: 3D profiles for $K = 6.3$ Pa·s^n, $n = 0.31$, and $\tau_o = 8$ Pa: (a) cuttings velocity and (b) cuttings concentration.

3.5. Annular Pressure Losses. Accurate estimation of annular pressure losses is very vital when designing drilling hydraulic programs, particularly the equivalent circulating densities (ECD) required for efficient transport of drilled cuttings from the wellbore to the surface. Figure 8 examines the influence of n, K, and τ_o on annular pressure loss. Figure 8(a) indicates that as the fluid becomes more shear-thinning, that is, $n < 1$, the pressure loss decreases. There is a gradual rise in pressure as loss from $n = 0.31$ to 0.51; however, a dramatic percentage increase of 316.4% is computed as n increased from 0.51 to 0.75. Furthermore, Figure 8(b) also reveals an increase in pressure loss as K increases from 1.7 to 6.3 Pa·s^n with approximately 132.6% increase in pressure loss. Last but not the least, increase in τ_o from 2 to 8 Pa had the least influence on pressure with nearly 13.6% increase.

4. Conclusions

A study on the effect of rheological parameters on cuttings transport velocity in YPL fluid flowing in eccentric narrow horizontal annulus is analyzed using Eulerian-Eulerian two-fluid CFD model. The proposed viscosity model for YPL fluid by Mendes and Dutra [37] was adopted since it is capable of avoiding numerical singularity difficulties at vanishing shear rate. For two-phase cuttings-YPL fluid flow, CFD calculated pressure loss data were validated using recent but rare experimental data from literature. The present model was used to analyze the effects of yield stress, consistency index, and flow behavior index of the carrier YPL fluid on cuttings transport velocity.

Within the context of this study, the radial distributions of cuttings transport velocity were observed in both wide and narrow annular regions. The increase in yield stress of the carrier fluid from 2 to 8 Pa did not have much influence on the cuttings transport velocity in the wide region especially in the core region. However, there was much improvement in the cuttings transport velocity at the vicinity of the walls, indicating less cuttings bed accumulation. In the narrow gap, cuttings travelled much faster in low yield stress fluids as a result of their low resistance to flow compared to high yield stress fluids.

The study also revealed that carrier fluids with high consistency index value enhanced more cuttings transport especially in the wide annular region due to the fluid's cuttings lifting ability. At the vicinity of the walls, cuttings travelled faster in low consistency index fluids due to the fluid's tendency to high shearing and, hence, resulted in less cuttings bed formation. In the narrow region, however, cuttings travelled faster in low consistency index fluids due to their less resistance to flow.

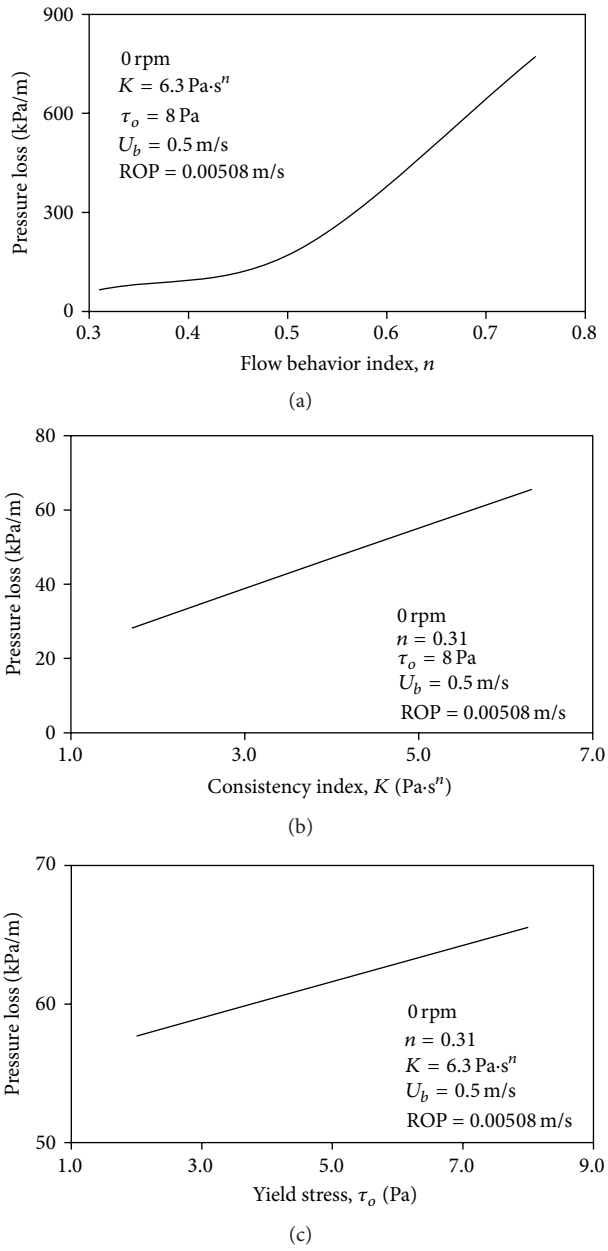

FIGURE 8: Effect of rheology on annular pressure loss: (a) flow behavior index, n, (b) consistency index, K, and (c) yield stress, τ_o.

Increasing the flow behavior index of the carrier fluid also showed much improvement in the cuttings transport velocity, especially in the core region of the wide annular gap. Meanwhile, carrier fluid with low flow behavior index transported cuttings better at the vicinity of the walls, an indication of less formation of cuttings bed. A reverse trend was, however, observed in the narrow annular gap, where there was significant cuttings transport in the carrier fluid with low flow behavior index. Three-dimensional flow distribution profiles have shown the actual dynamics of cuttings travelling in the eccentric annulus, where most of the cuttings were inclined to travel in the wide margin with less stress.

The YPL fluid model has been shown to fit much better rheological data of drilling fluids in the oil and gas industry compared to the Bingham plastic and power law fluid models. Furthermore, YPL fluids with high yield stress values reduce convective heat loss in most especially high temperature wellbores, thus possessing the very rheological properties which are important for an insulating fluid to perform well. It is noteworthy that YPL fluids have viscosities that increase significantly as shear-strain rate diminishes; hence, by increasing the viscosity of the fluid, the drilling engineer can gain partial control over convection heat loss. More importantly, YPL fluids tend to have relatively low viscosity at high shear rates (shear-thinning), making them easier to place initially, to bleed off pressure that may build up in the annulus equipped with venting capability, and to displace the drilling fluid in the event of well intervention. This study provides a guide to the drilling engineer on the selection of YPL fluid rheological properties which would enhance efficient transport of drilled cuttings in narrow horizontal wellbores.

It was further observed that the rheology of YPL fluids has significant effect on the annular pressure losses. Proper caution must be taken in selecting the fluid rheology to ensure efficient cuttings transport while maintaining a bottomhole pressure which will not fracture the formation.

Nomenclature

C_D: Drag coefficient (—)
d_s: Solid particle mean diameter (m)
D_i: Outer diameter of inner pipe (m)
D_o: Inner diameter of outer pipe (m)
D_h: Hydraulic diameter, $D_o - D_i$ (m)
e: Offset distance (m)
g: Gravity vector (m/s^2)
$\hbar_l$: Liquid phase volume fraction (—)
$\hbar_s$: Solid phase volume fraction (—)
K: Consistency index (Pa·s^n)
L: Annular geometry length (m)
L_h: Hydrodynamic length (m)
M: Interphase momentum transfer
M_d: Drag force per unit volume (N/m^3)
M_L: Lift force per unit volume (N/m^3)
n: Flow behavior index (—)
N_{Re}: Fluid Reynolds number (—)
N_{Re_p}: Solid particles Reynolds number (—)
N_{Re_ω}: Vorticity Reynolds number (—)
P_s: Solid particle pressure (Pa)
r: Radial direction
R: Normalized radial distance $((R_2 - r)/(R_2 - R_1))$
ROP: Rate of penetration (m/s)
u: Cuttings velocity at any radial distance (m/s)
U_b: Bulk fluid velocity (m/s)
U_l: Fluid phase velocity vector (m/s)
U_s: Solid phase velocity vector (m/s)
z: Axial direction.

Greek Symbols

ε: Eccentricity $(2e/(D_o - D_i))$
ρ_l: Fluid phase density (kg/m^3)
ρ_s: Solid phase density (kg/m^3)
$\bar{\bar{\tau}}$: Viscous stress tensor (Pa)
κ: Diameter ratio (D_i/D_o)
η_o: Zero shear rate viscosity (Pa·s)
η: Viscosity defined in (14) (Pa·s)
μ_l: Liquid viscosity (Pa·s)
μ_a: Apparent viscosity (Pa·s)
μ_r: Relative viscosity
μ_s: Solid viscosity (Pa·s)
μ_{susp}: Suspension viscosity (Pa·s)
υ: Specific volume (m^3/kg)
ω: Angular velocity (1/min)
$\dot{\gamma}$: Shear rate (1/s)
Ω: Rotation vector (1/min)
θ: Circumferential direction.

Competing Interests

The author declares that there are no competing interests regarding the publication of this paper.

References

[1] R. B. Adari, S. Miska, E. Kuru, P. Bern, and A. Saasen, "Selecting drilling fluid properties and flow rates for effective hole cleaning in high-angle and horizontal wells," in *Proceedings of the SPE Annual Technical Conference and Exhibition*, pp. 273–281, Dallas, Tex, USA, October 2000.

[2] A. Mihalakis, P. Makri, V. C. Kelessidis, G. Christidis, A. Foscolos, and K. Papanikolaou, "Improving rheological and filtration properties of drilling muds with addition of greek lignite," in *Proceedings of the 7th National Congress on Mechanics (HSTAM '04)*, Chania, Greece, 2004.

[3] R. Maglione, G. Robotti, and R. Romagnoli, "In-situ rheological characterization of drilling mud," *SPE Journal*, vol. 5, no. 4, pp. 377–386, 2000.

[4] R. Ahmed and S. Miska, *Experimental Study and Modeling of Yield Power-Law Fluid in Annuli with Drillpipe Rotation*, Society of Petroleum Engineers, Richardson, Tex, USA, 2008.

[5] V. C. Kelessidis, R. Maglione, C. Tsamantaki, and Y. Aspirtakis, "Optimal determination of rheological parameters for Herschel-Bulkley drilling fluids and impact on pressure drop, velocity profiles and penetration rates during drilling," *Journal of Petroleum Science and Engineering*, vol. 53, no. 3-4, pp. 203–224, 2006.

[6] K. Founargiotakis, V. C. Kelessidis, and R. Maglione, "Laminar, transitional and turbulent flow of Herschel-Bulkley fluids in concentric annulus," *Canadian Journal of Chemical Engineering*, vol. 86, no. 4, pp. 676–683, 2008.

[7] V. C. Kelessidis, P. Dalamarinis, and R. Maglione, "Experimental study and predictions of pressure losses of fluids modeled as Herschel-Bulkley in concentric and eccentric annuli in laminar, transitional and turbulent flows," *Journal of Petroleum Science and Engineering*, vol. 77, no. 3-4, pp. 305–312, 2011.

[8] O. Erge, E. M. Ozbayoglu, S. Z. Miska et al., *The Effects of Drillstring Eccentricity, Rotation, and Buckling Configurations on Annular Frictional Pressure Losses While Circulating Yield Power Law Fluids*, Society of Petroleum Engineers, 2014.

[9] A. Taghipour, B. Lund, J. D. Ytrehus et al., "Experimental study of friction and cutting transport in non-circular borehole geometry," in *Proceedings of the SPE/IADC Middle East Drilling Technology Conference & Exhibition*, pp. 821–835, Society of Petroleum Engineers, Dubai, UAE, October 2013.

[10] H. Cho, S. N. Shah, and S. O. Osisanya, "A three-segment hydraulic model for cuttings transport in horizontal and deviated wells," in *Proceedings of the SPE/Petroleum Society of CIM International Conference on Horizontal Well Technology*, SPE/PSCIM 65488, Calgary, Canada, 2000.

[11] S. G. Valluri, S. Z. Miska, R. Ahmed, M. Yu, and N. Takach, "Experimental study of effective hole cleaning using 'sweep' in horizontal wellbores," in *Proceedings of the SPE Annual Technical Conference and Exhibition*, SPE 101220, San Antonio, Tex, USA, 2006.

[12] M. Mohammadsalehi and N. Malekzadeh, "Optimization of hole cleaning and cutting removal in vertical, deviated and horizontal wells," in *Proceedings of the Asia Pacific Oil and Gas Conference and Exhibition*, SPE 143675, Society of Petroleum Engineers, Jakarta, Indonesia, September 2011.

[13] R. L. Horton, T. S. Froitland, W. E. Foxenberg, and D. A. Knox, "A new yield power law analysis tool improves insulating annular fluid design," in *Proceedings of the International Petroleum Technology Conference*, Doha, Qatar, November 2005.

[14] B. Bui, "Modeling the effect of pipe rotation on pressure loss through tool joint," in *Proceedings of the SPETT Energy Conference and Exhibition*, SPE-157982-MS, Society of Petroleum Engineers, Port-of-Spain, Trinidad, June 2012.

[15] T. N. Ofei, S. Irawan, W. Pao, and R. E. Osgouei, "Modified Yield Power-Law fluid flow in narrow annuli with inner rotating pipe," *Canadian Journal of Chemical Engineering*, vol. 93, no. 1, pp. 150–165, 2015.

[16] M. Mokhtari, M. Ermila, and A. N. Tutuncu, "Accurate bottomhole pressure for fracture gradient prediction and drilling fluid pressure program-part 1," in *Proceedings of the 46th U.S. Rock Mechanics/Geomechanics Symposium*, American Rock Mechanics Association, Chicago, Ill, USA, June 2012.

[17] T. N. Ofei, S. Irawan, and W. Pao, "CFD method for predicting annular pressure losses and cuttings concentration in eccentric horizontal wells," *Journal of Petroleum Engineering*, vol. 2014, Article ID 486423, 16 pages, 2014.

[18] X.-H. Zhu, C. Sun, and H. Tong, "Distribution features, transport mechanism and destruction of cuttings bed in horizontal well," *Journal of Hydrodynamics*, vol. 25, no. 4, pp. 628–638, 2013.

[19] L.-C. Qiu and C.-Y. Wu, "A hybrid DEM/CFD approach for solid-liquid flows," *Journal of Hydrodynamics*, vol. 26, no. 1, pp. 19–25, 2014.

[20] S.-M. Han, Y.-K. Hwang, N.-S. Woo, and Y.-J. Kim, "Solid-liquid hydrodynamics in a slim hole drilling annulus," *Journal of Petroleum Science and Engineering*, vol. 70, no. 3-4, pp. 308–319, 2010.

[21] S. A. Hashemi, A. Sadighian, S. I. A. Shah, and R. S. Sanders, "Solid velocity and concentration fluctuations in highly concentrated liquid-solid (slurry) pipe flows," *International Journal of Multiphase Flow*, vol. 66, pp. 46–61, 2014.

[22] J. Capecelatro and O. Desjardins, "Eulerian-Lagrangian modeling of turbulent liquid-solid slurries in horizontal pipes," *International Journal of Multiphase Flow*, vol. 55, pp. 64–79, 2013.

[23] M. Eesa and M. Barigou, "Horizontal laminar flow of coarse nearly-neutrally buoyant particles in non-Newtonian conveying fluids: CFD and PEPT experiments compared," *International Journal of Multiphase Flow*, vol. 34, no. 11, pp. 997–1007, 2008.

[24] Z.-M. Wang, X.-L. Guo, M. Li, and Y.-K. Hong, "Effect of drillpipe rotation on borehole cleaning for extended reach well," *Journal of Hydrodynamics*, vol. 21, no. 3, pp. 366–372, 2009.

[25] K. Ekambara, R. S. Sanders, K. Nandakumar, and J. H. Masliyah, "Hydrodynamic simulation of horizontal slurry pipeline flow using ANSYS-CFX," *Industrial and Engineering Chemistry Research*, vol. 48, no. 17, pp. 8159–8171, 2009.

[26] X. Sun, K. Wang, T. Yan, S. Shao, and J. Jiao, "Effect of drillpipe rotation on cuttings transport using computational fluid dynamics (CFD) in complex structure wells," *Journal of Petroleum Exploration and Production Technology*, vol. 4, no. 3, pp. 255–261, 2014.

[27] T. N. Ofei, S. Irawan, and W. Pao, "Modelling of pressure drop in eccentric narrow horizontal annuli with the presence of cuttings and rotating drillpipe," *International Journal of Oil, Gas and Coal Technology*, vol. 9, no. 1, pp. 39–60, 2015.

[28] M. Sommerfeld and S. Lain, "Parameters influencing dilute-phase pneumatic conveying through pipe systems: a computational study by the Euler/Lagrange approach," *Canadian Journal of Chemical Engineering*, vol. 93, no. 1, pp. 1–17, 2015.

[29] B. G. M. van Wachem and A. E. Almstedt, "Methods for multiphase computational fluid dynamics," *Chemical Engineering Journal*, vol. 96, no. 1–3, pp. 81–98, 2003.

[30] C. Y. Wen and Y. H. Yu, "Mechanics of fluidization," *Chemical Engineering Progress Symposium Series*, vol. 62, pp. 100–111, 1966.

[31] D. Gidaspow, *Multiphase Flow and Fluidization*, Academic Press, Boston, Mass, USA, 1994.

[32] P. G. Saffman, "The lift on a small sphere in a slow shear flow," *Journal of Fluid Mechanics*, vol. 22, no. 2, pp. 385–400, 1965.

[33] P. G. Saffman, "The lift on a small sphere in a slow shear flow—corrigendum," *Journal of Fluid Mechanics*, vol. 31, no. 03, p. 624, 1968.

[34] R. Mei and J. F. Klausner, "Shear lift force on spherical bubbles," *International Journal of Heat and Fluid Flow*, vol. 15, no. 1, pp. 62–65, 1994.

[35] D. G. Thomas, "Transport characteristics of suspension: VIII. A note on the viscosity of Newtonian suspensions of uniform spherical particles," *Journal of Colloid Science*, vol. 20, no. 3, pp. 267–277, 1965.

[36] A. Einstein, "Eine neue Bestimmung der Moleküldimensionen [AdP 19, 289 (1906)]," *Annalen der Physik*, vol. 14, supplement 1, pp. 229–247, 2005.

[37] P. R. S. Mendes and S. S. E. Dutra, "A viscosity function for viscoplastic liquids," *Annual Transactions of the Nordic Rheology Society*, vol. 12, pp. 183–188, 2004.

[38] Y. Cengel and J. A. Cimbala, *Fluid Mechanics: Fundamentals and Applications*, McGraw-Hill Higher Education, 2004.

[39] C. M. Rhie and W. L. Chow, "Numerical study of the turbulent flow past an airfoil with trailing edge separation," *AIAA Journal*, vol. 21, no. 11, pp. 1525–1532, 1983.